Acta Crystallographica Section D
Biological Crystallography
ISSN 0907-4449

Plant multifunctional nuclease TBN1 with unexpected phospholipase activity: structural study and reaction-mechanism analysis

Tomáš Koval',[a,b]* Petra Lipovová,[c] Tomáš Podzimek,[c] Jaroslav Matoušek,[d] Jarmila Dušková,[b] Tereza Skálová,[b] Andrea Štěpánková,[b] Jindřich Hašek[b] and Jan Dohnálek[a,b]*

[a]Institute of Macromolecular Chemistry, AS CR, v.v.i., Heyrovskeho nam. 2, 162 06 Praha 6, Czech Republic, [b]Institute of Physics AS CR, v.v.i., Na Slovance 2, 182 21 Praha 8, Czech Republic, [c]Institute of Chemical Technology, Technická 5, 166 28 Praha 6, Czech Republic, and [d]Institute of Plant Molecular Biology, Biology Centre, AS CR, v.v.i., Branišovská 31, 370 05 České Budějovice, Czech Republic

Correspondence e-mail: koval.tomas@gmail.com, dohnalek007@gmail.com

Received 5 September 2012
Accepted 22 October 2012

PDB References: TBN1, wild type, 3sng; N211D mutant, 4dj4

Type I plant nucleases play an important role in apoptotic processes and cell senescence. Recently, they have also been indicated to be potent anticancer agents in *in vivo* studies. The first structure of tomato nuclease I (TBN1) has been determined, its oligomerization and activity profiles have been analyzed and its unexpected activity towards phospholipids has been discovered, and conclusions are drawn regarding its catalytic mechanism. The structure-solution process required X-ray diffraction data from two crystal forms. The first form was used for phase determination; the second form was used for model building and refinement. TBN1 is mainly α-helical and is stabilized by four disulfide bridges. Three observed oligosaccharides are crucial for its stability and solubility. The active site is localized at the bottom of the positively charged groove and contains a zinc cluster that is essential for enzymatic activity. An equilibrium between monomers, dimers and higher oligomers of TBN1 was observed in solution. Principles of the reaction mechanism of the phosphodiesterase activity are suggested, with central roles for the zinc cluster, the nucleobase-binding pocket (Phe-site) and Asp70, Arg73 and Asn167. Based on the distribution of surface residues, possible binding sites for dsDNA and other nucleic acids with secondary structure were identified. The phospholipase activity of TBN1, which is reported for the first time for a nuclease, significantly broadens the substrate promiscuity of the enzyme, and the resulting release of diacylglycerol, which is an important second messenger, can be related to the role of TBN1 in apoptosis.

1. Introduction

Tomato nuclease TBN1 from *Solanum lycopersicum* (EC 3.1.30.*x*; UniProt sequence accession No. Q0KFV0; gene name *tbn*1; Matousek *et al.*, 2007) is a Zn^{2+}-dependent member of the plant nuclease I family composed of 277 amino acids with a protein molecular mass of 31.6 kDa (about 37 kDa when fully glycosylated) and with three N-glycosylation sites. Enzymes from the plant nuclease I family are Zn^{2+}-, Mg^{2+}- or Ca^{2+}-dependent, have a preference for bonds adjacent to adenine, produce 5′-mononucleotides as end products at pH optima in the range 5.0–6.5, are able to cleave different homopolymers and are sensitive to ethylenediaminetetraacetic acid (EDTA). Their molecular masses are in the range 31–37 kDa and they are related to fungal P1 and S1 nucleases (Pérez-Amador *et al.*, 2000). TBN1 cleaves RNA and DNA in both single-stranded and double-stranded forms and also shows 3′-nucleotidase activity (the term 'bifunctional' historically originates from this dual activity and becomes obsolete with the findings of this work; nevertheless, the name 'TBN1' will be preserved for consistency with previous work). The enzyme

Table 1
Optimized crystallization conditions yielding the crystals of R-TBN1wt and R-TBN1-N211D used for X-ray diffraction data collection.

	Reservoir-solution composition	Growth time	Typical crystal dimensions (μm)
R-TBN1wt	1.0 *M* ammonium sulfate, 0.1 *M* bis-tris pH 5.5, 1%(*w*/*v*) PEG 3350 (Index No. 32)	One year	500 × 70 × 70
R-TBN1-N211D	0.16 *M* $MgCl_2$, 0.08 *M* Tris–HCl pH 8.5, 19%(*w*/*v*) PEG 3350, 3.3%(*v*/*v*) 1,4-butanediol	One week	600 × 100 × 100

acts as a phosphodiesterase, cleaving the P—O3′ bonds in nucleic acids. TBN1 plays a significant role in specific apoptotic functions and in plant-tissue differentiation, vascular-system development and viroid pathogenesis (Matousek *et al.*, 2007). Its activity towards a proliferation of tumours has been demonstrated *in vivo* on athymic *nu*/*nu* mice bearing human melanoma, human prostatic tumours and human neuroblastoma (Matousek *et al.*, 2009, 2010).

The activity of TBN1 against multiple types of nucleic acids (NAs), including structured DNA and RNA and homopolymers, raises questions regarding its key factors enabling the binding and cleavage of double strands and higher NA structures. The contrast is even greater when, for example, P1 nuclease with a related sequence exhibits only minute activity towards dsDNA (Volbeda *et al.*, 1991; Romier *et al.*, 1998). The mechanism of the catalytic hydrolysis of NA has not been fully explained and is very likely to differ among the individual types of DNases and nucleases utilizing two or three metal ions. In this study, we focus on the structure–function relationship in plant nucleases of type I and draw some conclusions regarding the catalytic mechanism and the *in vitro* and *in vivo* properties of this enzyme.

2. Materials and methods

2.1. Expression and purification

For crystallization and diffraction experiments, recombinant tomato nuclease I (R-TBN1) was used. Two variants of TBN1 were studied: the wild type (R-TBN1wt) and a mutated version in which Asn211 was replaced by Asp (R-TBN1-N211D). This mutation leads to a hypoglycosylated version of the enzyme with only two N-glycosylation sites. Both proteins were prepared by insertion of cDNA (UniProt sequence accession No. Q0KFV0, including the signal-peptide region) into the plant expression vector pLV07 (Matousek *et al.*, 2009; plasmid clone 3062 in the case of the N211D mutant) and by using *Agrobacterium tumefaciens* leaf disc infiltration and expression in *Nicotiana benthamiana* leaves. The enzyme was purified by ammonium sulfate precipitation, ion-exchange chromatography using a HiTrap Q FF column (Amersham Biosciences) and affinity chromatography on HiTrap Heparin HP (Amersham Biosciences), and was desalted on a PD-10 column (Amersham Biosciences). The details of the procedure have been described previously (Lipovova *et al.*, 2008; Matousek *et al.*, 2009). R-TBN1wt was stored in 50 m*M* Tris–HCl pH 7.5, 0.3 *M* NaCl. R-TBN1-N211D was stored in the same buffer with the addition of 1%(*v*/*v*) glycerol and 10 m*M* 3-(1-pyridino)-1-propanesulfonate (NDSB-201).

2.2. Modification of surface properties

Selective reductive methylation of R-TBN1wt surface lysine residues was performed using the commercially available JBS Methylation Kit (Jena Bioscience, Jena, Germany) according to the user-guide protocol (Kim *et al.*, 2008). Deglycosylation of R-TBN1wt was performed using PNGase F (Sigma–Aldrich, St Louis, Missouri, USA) using a method similar to that described previously (Podzimek *et al.*, 2011).

2.3. Crystallization

For crystallization, both R-TBN1wt and R-TBN1-N211D were used in the storage buffers mentioned above. R-TBNwt was concentrated to 4 mg ml^{-1}. In addition to the orthorhombic and rhombohedral crystals of R-TBN1wt obtained previously (Koval' *et al.*, 2011), trigonal crystals of R-TBN1wt were found in condition No. 32 (Table 1) of the Index screen (Hampton Research) one year after initial setup. The hanging-drop vapour-diffusion method was used at 291 K with a 1:1 volume ratio of protein solution to reservoir solution in the drop (0.5 μl + 0.5 μl). Crystallization of R-TBN1-N211D began with testing and further optimization of the successful and promising conditions previously used to crystallize R-TBN1wt (Dohnálek *et al.*, 2011; Koval' *et al.*, 2011). R-TBN1-N211D was concentrated to only 2 mg ml^{-1} because of its slightly lower solubility in comparison to the wild-type enzyme. The best crystals were obtained using an optimized condition based on solution No. 85 of the Index screen (Hampton Research) and the hanging-drop vapour-diffusion method (Table 1). A drop was formed by mixing 0.5 μl protein solution with 0.5 μl reservoir solution.

2.4. X-ray diffraction analysis and structure solution

Crystals of R-TBN1-N211D were equilibrated for 15 s in mother solution with glycerol added to a concentration of 20%(*v*/*v*) as a cryoprotectant. The R-TBN1wt crystals were retrieved from crystallization drops one year after setup and according to the observed mother-solution behaviour, the concentration of ammonium sulfate was close to the saturation level. Therefore, there was no need for cryoprotectant in this case. Crystals of both types were mounted in nylon CryoLoops (Hampton Research) and quickly vitrified in liquid nitrogen. Data were collected from both crystal types at 100 K on BL14.1 of the BESSY II synchrotron-radiation source, Helmholtz-Zentrum Berlin using a MAR Mosaic CCD 225 detector and a mini kappa goniometer (Mueller *et al.*, 2012). The best crystal of R-TBN1wt diffracted to 2.16 Å resolution and the best crystal of R-TBN1-N211D diffracted to 2.35 Å resolution. The data were processed using *HKL*-2000 (Otwinowski & Minor, 1997) and the data statistics are summarized in Table 2.

Table 2
Data-collection statistics and structure-refinement parameters for R-TBN1wt and R-TBN1-N211D.

Values in parentheses are for the highest resolution shell.

	R-TBN1wt	R-TBN1-N211D
Data-collection statistics		
Wavelength (Å)	0.91841	0.91841
Crystal-to-detector distance (mm)	240	288
No. of oscillation images processed	180	180
Exposure time per image (s)	15	5
Oscillation width (°)	1.0	1.0
Space group	$P3_121$	$H3$
Unit-cell parameters (Å)	$a = b = 101.0$, $c = 71.5$	$a = b = 113.3$, $c = 138.3$
Resolution range (Å)	35–2.16 (2.24–2.16)	35–2.35 (2.41–2.35)
No. of observations	256484	153947
No. of unique reflections	23098 (2280)	26874 (1524)
Overall multiplicity ($I^+ = I^-$)	11.3 (11.1)	5.7 (4.7)
Data completeness (%)	100.0 (100.0)	97.8 (78.5)
Mosaicity (°)	0.3	0.6
Average $I/\sigma(I)$	26.7 (4.5)	17.7 (2.3)
R_{merge}	0.094 (0.597)	0.098 (0.615)
$R_{r.i.m.}$†	0.122 (0.760)	0.109 (0.699)
Structure-refinement parameters		
R_{work}	0.180	0.183
R_{free}	0.223	0.207
R_{all}	0.188	0.186
Average B factor (Å^2)	31.6	40.6
R.m.s.d. from ideal		
Bond lengths (Å)	0.015	0.012
Bond angles (°)	1.57	1.46
Solvent content (%)	63	55
Matthews coefficient (Å^3 Da^{-1})	3.3	2.7
No. of non-H atoms	2441	4540
No. of protein monomers per asymmetric unit	1	2
Modelled amino-acid residues	26–292	Chain *A*, 26–291; chain *B*, 26–131, 136–215, 226–290
No. of water molecules	140	169
Modelled oligosaccharides	Asn119 and Asn211, GlcNAc-(4→1)-GlcNAc-(4→1)-β-D-Man; Asn137, GlcNAc-(4→1)-GlcNAc-(4→1)-β-D-Man-(6→1)-α-D-Man	Asn119(*A*), GlcNAc-(4→1)-GlcNAc; Asn119(*B*), GlcNAc-(4→1)-GlcNAc-(4→1)-β-D-Man-(3→1)-α-D-Man; Asn137, GlcNAc-(4→1)-GlcNAc-(4→1)-β-D-Man-(3→1)-α-D-Man (6→1)-α-D-Man
Other modelled moieties	3 Zn^{2+}, 1 Cl^-, 1 SO_4^{2-}, 1 bis-tris	6 Zn^{2+}, 2 Cl^-, 1 Na^+

The phase problem was previously solved by MAD phasing using Zn^{2+} ions natively present in the enzyme, data from the rhombohedral crystal of R-TBN1wt (Koval' *et al.*, 2011) and the programs *SHELXC*, *SHELXD* and *SHELXE* (Sheldrick, 2008). A preliminary structure model was built by placing the P1 nuclease structure (PDB entry 1ak0; Romier *et al.*, 1998) into experimental electron density from this MAD experiment using *MOLREP* (Vagin & Teplyakov, 2010) from the *CCP*4 suite (Winn *et al.*, 2011). The low quality of the data from the rhombohedral crystal allowed only limited refinement of the model (Dohnálek *et al.*, 2011; Koval' *et al.*, 2011). This 'incomplete' model was used for the molecular-replacement (MR) solution of the phase problem for the data set from the trigonal crystal of R-TBN1wt (Table 2) using *MOLREP* (Vagin & Teplyakov, 2010). The initially placed model in the R-TBN1wt unit cell resulted in an R_{cryst} of 0.585 and a contrast of 17.8 without any packing conflicts.

The structure of the hypoglycosylated mutant R-TBN1-N211D was solved by MR using *MOLREP* (Vagin & Teplyakov, 2010) with the finalized model of R-TBN1wt as a search model. The MR procedure resulted in a solution with an initial R_{cryst} of 0.405 and a contrast of 6.2.

Both structures were built using *Coot* (Emsley & Cowtan, 2004) and refined in *REFMAC*5 (Murshudov *et al.*, 2011). R_{free} (5.1% of the reflections in the case of R-TBN1wt and 5.0% in the case of R-TBN1-N211D) was used as a cross-validation method during refinement. Structure quality was assessed using a set of validation tools in *Coot* (Emsley & Cowtan, 2004) and also the remote validation services provided by the *MolProbity* program suite (Chen *et al.*, 2010). 95.5% of the R-TBN1wt residues were in the favoured regions of the Ramachandran plot; there were no outliers. 95.3% of the R-TBN1-N211D residues were in the favoured regions of the Ramachandran plot; there was one outlier (Thr131, chain *A*) supported by electron density.

The structures of R-TBN1wt and R-TBN1-N211D were deposited in the PDB with codes 3sng and 4dj4, respectively. The refinement statistics are summarized in Table 2.

2.5. Surface electrostatic potential distribution and docking calculations

The surface electrostatic potential distribution was calculated for protonation states at pH 6, which is close to the pH optimum of activity (Podzimek *et al.*, 2011). The calculations were performed using *APBS* (Baker *et al.*, 2001) and a parameter file created by *PDB2PQR* 1.8 (Dolinsky *et al.*, 2004). Protonation states were assigned by *PropKa* (Li *et al.*, 2005). Docking of 5′-AMP and 3′-AMP into the active site was performed using *AutoDock Vina* (Trott & Olson, 2010). A search for possible binding modes of dsDNA to the active site was performed using *ParaDock* (Banitt & Wolfson, 2011).

2.6. Oligomerization of R-TBN1wt and R-TBN1-N211D in solution

The oligomerization state and behaviour of R-TBN1 samples in solution were tested by dynamic light scattering (DLS) and size-exclusion chromatography. DLS experiments

were performed using a Zetasizer Nano (Malvern Instruments) and a 45 µl quartz cuvette. All measurements were performed at 291 K with a protein concentration of 1 mg ml^{-1}.

Size-exclusion chromatography was performed using HiLoad Superdex 200 prep-grade and HiLoad Superdex 75 prep-grade columns and an ÄKTApurifier 10 system (GE Healthcare) calibrated using protein standards. All samples were run in 0.05 *M* Tris–HCl pH 7.5, 0.15 *M* NaCl.

2.7. Detection of phospholipase activity

The phospholipase C-like activity of R-TBNwt was tested using two independent experiments. The first was based on the cleavage of *p*-nitrophenylphosphorylcholine (*p*-NPPC), an artificial substrate for the detection of phospholipase C activity (Kurioka & Matsuda, 1976). In the first experiment, the reaction mixture (100 µl) consisted of 9 m*M* *p*-NPPC (9 µl), 1.5 µg TBN1 (10 µl at 0.15 mg ml^{-1}) and the reaction was performed in 50 m*M* Tris–malate buffer pH 7.3 (81 µl) at 310 K for 0.5, 1, 2, 3 and 4 h. The reaction was stopped by adding 100 µl 10%(*w*/*v*) Na_2CO_3. The absorbance of the released *p*-nitrophenol was measured at λ = 410 nm and its concentration was calculated from a calibration curve (20–100 µ*M*). The specific activity of TBN1 with *p*-NPPC was expressed as picomoles of *p*-nitrophenol released by 1 µg of TBN1 after 1 min (pmol min^{-1} µg^{-1}).

The second assay was performed according to a protocol from the Sigma–Aldrich Corporation (St Louis, Missouri, USA) based on the cleavage of L-α-phosphatidylcholine (L-α-lecithin) into 1,2-diglyceride and choline phosphate by an enzyme with phospholipase C activity (Kurioka & Liu, 1967). The reaction mixture contained 10 µg TBN1. The reaction was performed in 50 m*M* Tris–malate pH 7.3 at 310 K for 20 min. Inorganic phosphate (P_i) was subsequently produced by alkaline phosphatase from *Escherichia coli* and detected using the Ames Colour Reagent (Barrows *et al.*, 1985) and absorption spectroscopy at λ = 660 nm.

2.8. Nuclease activity

Specific activities of native and methylated R-TBN1wt and R-TBN1-N211D towards dsDNA (calf thymus; Calbiochem), ssDNA (heat-denatured) and RNA (yeast; Worthington) were measured using an assay formulated previously by Podzimek *et al.* (2011). The enzymes were in 50 m*M* Tris–HCl pH 7.5 for these experiments. Each reaction solution was composed of 50 µl 50 m*M* NaH_2PO_4/Na_2HPO_4 buffer pH 6.2, 50 µl 1 µg µl^{-1} substrate solution (dsDNA, ssDNA or RNA) and a defined quantity of protein sample to give a total volume of 105 µl. The reaction was carried out at 310 K for 5 min and was stopped by the addition of 300 µl 96%(*v*/*v*) ethanol and 10 µl 3 *M* sodium acetate pH 5.2. The reaction mixture was equilibrated for 20 min at 253 K and then centrifuged for 15 min at 277 K and 22 000*g*. The products of the reaction were detected in the supernatant by absorption spectroscopy at 260 nm.

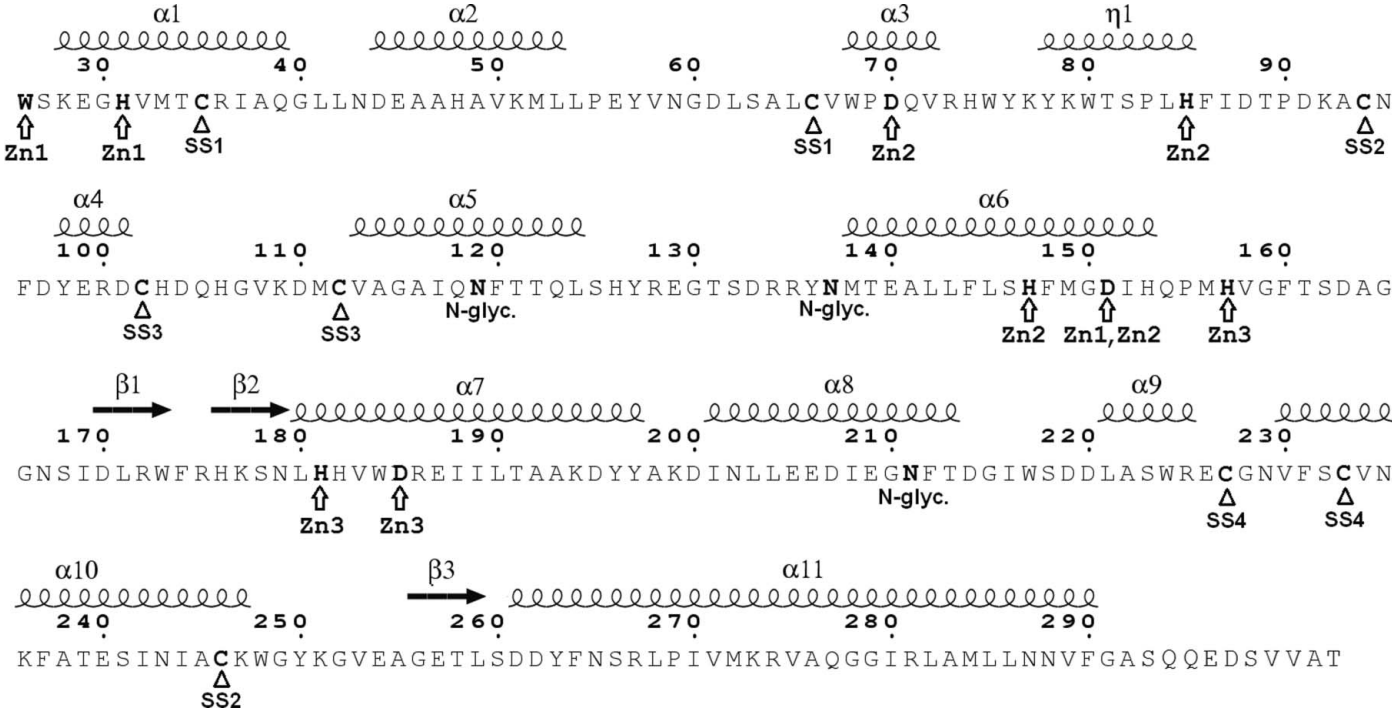

Figure 1
Amino-acid sequence of mature R-TBN1wt with structural features marked. Secondary-structure elements are labelled by letters of the Greek alphabet: α-helices are labelled α1–α11, β-strands β1–β3 and the 3_{10}-helix η1. Residues coordinating Zn^{2+} ions are marked by arrows, cysteine residues participating in disulfide bridges are labelled and marked by triangles and glycosylation sites are labelled.

Table 3
Coordinating atoms and bond distances for Zn^{2+} ions in the active site of R-TBN1wt and R-TBN1-N211D.

(i) R-TBNwt, symmetry operator $-x + y - 1, -x - 1, z - 1/3$. (ii) R-TBN1-N211D, both chains. (iii) R-TBN1wt. (iv) Asp133 $O^{\delta2}$ from chain *A* coordinates Zn3 from chain *B*.

		Distance (Å)		
Zn^{2+}	Coordinating atom	R-TBN1wt	R-TBN1-N211D, chain *A*	R-TBN1-N211D, chain *B*
Zn1	Trp26 N	2.2	2.0	2.2
	Trp26 O	2.2	2.3	2.3
	His31 N^{ε}	2.0	2.0	1.8
	Asp151 $O^{\delta1}$	2.1	2.1	2.0
	W701	1.9	2.1	1.8
Zn2	His85 $N^{\delta1}$	2.1	2.2	2.3
	Asp70 O^{ε}	2.7	2.5	2.7
	His147 N^{ε}	2.0	2.1	2.1
	Asp151 $O^{\delta2}$	2.0	2.2	2.2
	W701	1.9	2.0	2.3
	W703	—	2.5	2.1
Zn3	His157 N^{ε}	2.1	2.2	2.2
	His181 N^{ε}	2.1	2.0	2.1
	Asp185 $O^{\delta2}$	2.1	2.0	2.1
	Ser132 O^{γ} (i), W702 (ii)	2.3	2.3	2.3
	SO_4^{2-} O^1 (iii), Asp133 $O^{\delta2}$ (iv)	2.1	—	2.3
	Ser132 O (i)	2.6	—	—

3. Results

3.1. Overall structural properties of TBN1

TBN1 has a phospholipase C-like/P1 nuclease fold built of 11 α-helices from four to 30 amino acids long (which include 51.6% of all residues), one eight-residue 3_{10}-helix and one small β-sheet composed of three four-residue strands in the order $\beta2$–$\beta1$–$\beta3$. $\beta1$ and $\beta3$ are parallel, with $\beta2$ antiparallel to them. Residues 26–292 are localized in the wild-type structure, with Trp26 being the first residue after the cleaved 25-residue signal sequence. The TBN1 fold is stabilized by four disulfide bridges. There are three N-glycosylation sites available on the surface of wild-type TBN1: Asn119, Asn137 and Asn211. Each site is occupied by an oligosaccharide including two units of *N*-acetylglucosamine (GlcNAc), one unit of β-D-mannose and two consecutive units of α-D-mannose. Two units of GlcNAc were always identified and modelled for all of the glycosylation sites. The number of localized mannose units varies and the complete composition of the glycans is not known. The overall structural features of TBN1 are illustrated on the amino-acid sequence in Fig. 1 and the structure is shown in Fig. 2(*a*). The surface electrostatic potential distribution, calculated at pH 6, clearly shows the positively charged active-site groove on the surface of the molecule (Fig. 2*b*).

3.1.1. Active site: catalytic Zn^{2+} cluster. The active site is located at the bottom of the wide positively charged groove on the surface of the molecule. The centre of the active site is formed by amino-acid residues coordinating three Zn^{2+} ions (Zn1, Zn2 and Zn3) arranged in a nearly right-angled triangle with a Zn2—Zn1—Zn3 angle of 91.2°. The distance between Zn1 and Zn2 is 3.3 Å. Zn3 is 4.8 Å from Zn1 and 5.9 Å from Zn2. The identity of the metal ions present in the active site was confirmed previously by an X-ray fluorescence measurement and the MAD technique (Dohnálek *et al.*, 2011; Kovaľ *et al.*, 2011). Each zinc ion is coordinated by two N atoms and three or four O atoms (Fig. 2*c*). Zn1 and Zn2 are placed deeper than Zn3 and form four coordination bonds to the surrounding amino acids and one or two to water molecules. Zn1 forms five coordination bonds in both structures, four of them to Trp26 (the N-terminus of the mature enzyme), His31 and Asp151. The fifth coordinating atom is the water molecule (hydroxide ion) W701 bridging Zn1 and Zn2. Zn2 has five (R-TBN1wt) or six (R-TBN1-N211D) coordination bonds, four to Asp70, His85, His147 and Asp151, one to W701 and, in the case of R-TBN1-N211D, also one to W703. Zn3 is more exposed to solvent and forms only three coordination bonds to TBN1 residues His157, His181 and Asp185. The other two (R-TBN1-N211D) or three (R-TBN1wt) coordination bonds are formed to water molecules or ligands. The Zn^{2+} ions connect distant parts of the protein chain, and in this way stabilize the fold of TBN1. The atoms coordinating Zn^{2+} ions and the bond distances in the R-TBN1wt and R-TBN1-N211D structures are summarized in Table 3 and are shown in Figs. 2(*c*) and 2(*d*).

3.1.2. Crystal packing. The crystal packing of both R-TBN1wt and R-TBN1-N211D is based on 'super-helices' composed of TBN1 molecules, with a helix pitch equal to three molecules. In both cases, the major interaction responsible for the formation of this superstructure is the binding of the loop SDR132–134 (Ser132, Asp133 and Arg134) of TBN1 into the active site of the next molecule in the super-helix. Interestingly, the loop–active site contacts in the wild-type and N211D mutant structures are similar but not entirely equal. In both cases Arg134 binds between Ala164 and Phe86 into the assumed nucleobase-binding site (Phe-site; see §4) *via* stacking interactions with the Phe86 side chain and the Ala164 main chain and also *via* hydrogen bonds to Asp88 (Fig. 2*e*). The differences are in the position of Arg134 in the Phe-site and in the hydrogen-bonding pattern. The second interaction of the SDR loop is the binding of Ser132 (in R-TBN1wt) or Asp133 (R-TBN1-N211D) to Zn3. These differences are most likely to be caused by the presence of a sulfate ion in the active site of R-TBN1wt. This ion enhances the SDR loop interaction in comparison with the sulfate-free structure of the N211D mutant. Details of both interactions are shown in Figs. 2(*f*) and 2(*g*).

3.2. Other structural details: R-TBN1wt

One SO_4^{2-} ion per molecule binds in the active site originating from ammonium sulfate present in the crystallization condition. A water molecule (or hydroxide ion) W701 is bound in the active site between Zn1 and Zn2. A Cl^- ion bridges Trp68 N^{ε} and an N atom of the second GlcNAc unit of the oligosaccharide at Asn137. One molecule of bis-tris (crystallization buffer) was modelled into electron density on R-TBN1 surface and was involved in a hydrophobic interaction with Phe231. Electron density was not observed for the

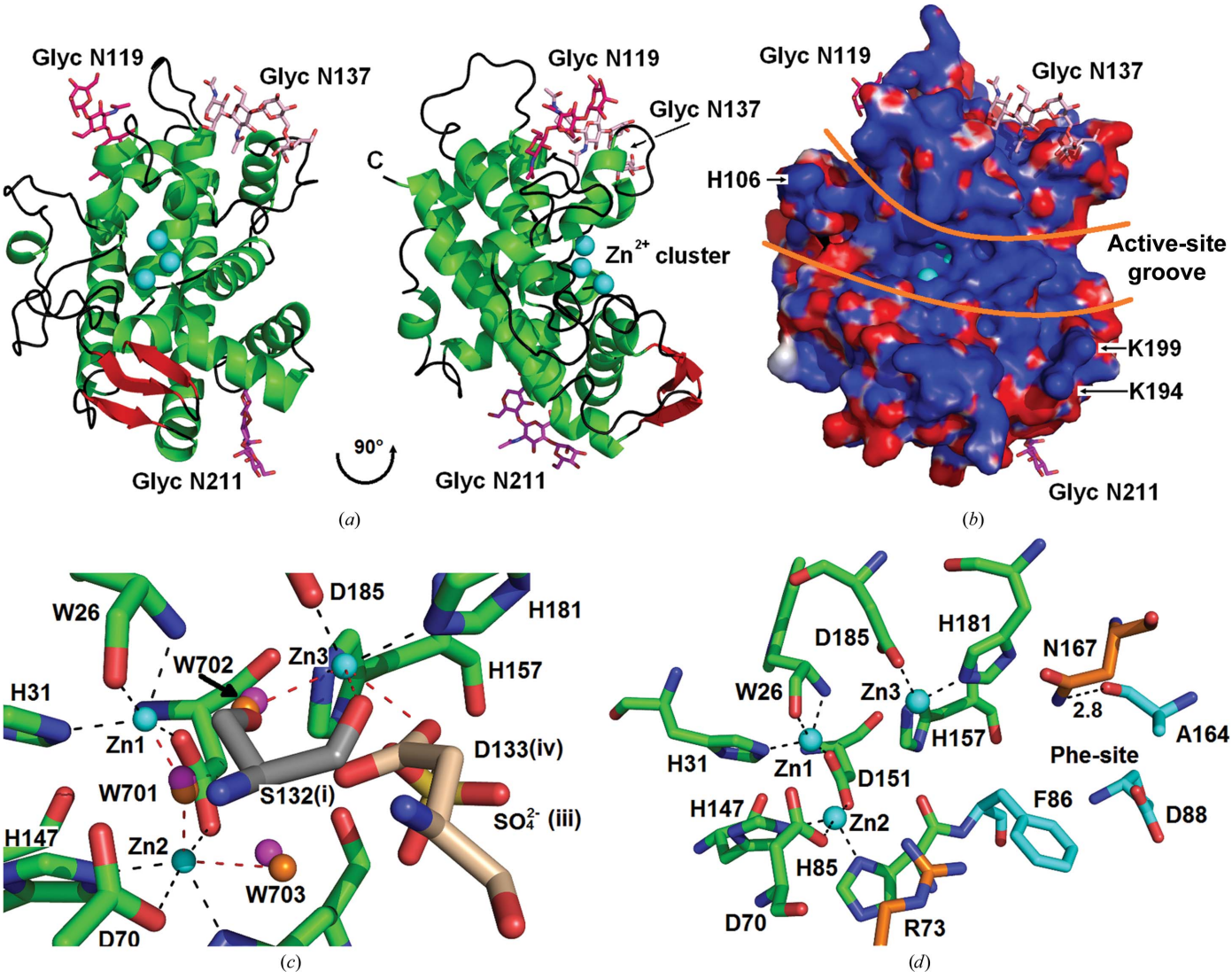

Figure 2
(*a*) Fold, secondary structure and main features of R-TBN1wt. Helices are coloured green and β-strands red. Zn^{2+} ions in the centre of the active site are shown as pale blue spheres. Glycans on the surface of the enzyme are shown as magenta sticks and labelled according to the modified residue. (*b*) Surface electrostatic potential distribution of TBN1 for the protonation state at pH 6. The orientation of the molecule is similar to that in (*a*), with the Zn^{2+} cluster in its centre. (*c*) Superposition of three independent structures (R-TBN1wt and R-TBN-N211D chain *A* and chain *B*) to describe the coordination of zinc ions in the TBN1 active site. Each Zn^{2+} is coordinated by two N atoms and three or four O atoms. Each coordinating atom position is conserved. The positions of W703 and Ser132 O can be vacant; all other positions are occupied in all structures. Superposition was performed by alignment of the zinc clusters; therefore, only Zn^{2+} ions (light blue spheres) and coordinating residues (green) from the R-TBNwt structure are shown. One water (hydroxide) in position W701, one SO_4^{2-} ion (iii) and Ser132 (i) (symmetry operator $-x+y-1, -x-1, z-1/3$) belong to R-TBN1wt. Waters in the W701, W702 and W703 positions represented by orange (chain *A*) and magenta (chain *B*) spheres belong to R-TBN1-N211D, together with Asp133 (iv) (Asp133 $O^{\delta 2}$ from chain *A* coordinates Zn3 from chain *B*). (i), (iii) and (iv) have the same meaning as in Table 3. (*d*) Overall features of the R-TBN1wt active site. Residues involved in coordination of Zn^{2+} ions are coloured green. Residues forming the nucleobase-binding pocket (Phe-site) are coloured pale blue. Two additional residues which are presumably involved in the reaction mechanism are coloured orange.

last ten amino-acid residues of the C-terminus and these were not modelled.

3.3. Other structural details: R-TBN1-N211D

The structure of the main chain of R-TBN1-N211D is very similar to that of the wild type, with a positional root-mean-square deviation (r.m.s.d.) of C^{α} atoms of 0.41 Å (chain *A* of R-TBN1-N211D, 264 residues aligned using *PDBeFold*; Krissinel & Henrick, 2004). In the R-TBN1-N211D structure a dimer is present in the asymmetric unit. Two regions in molecule *B* of the dimer (loops 132–135 and 217–225) cannot be modelled owing to disorder. Nevertheless, both loops are well localized in the case of chain *A*. In contrast to R-TBN1wt, there are three water molecules bound in the first coordination sphere of the zinc ions in the active site of R-TBN1-N211D (further described as in chain *A* of the dimer). W701 bridges Zn1 and Zn2, similarly as in R-TBN1wt. The other two zinc ions are not present in the wild-type structure. W702 coordinates Zn3 and participates in a hydrogen bond to W701.

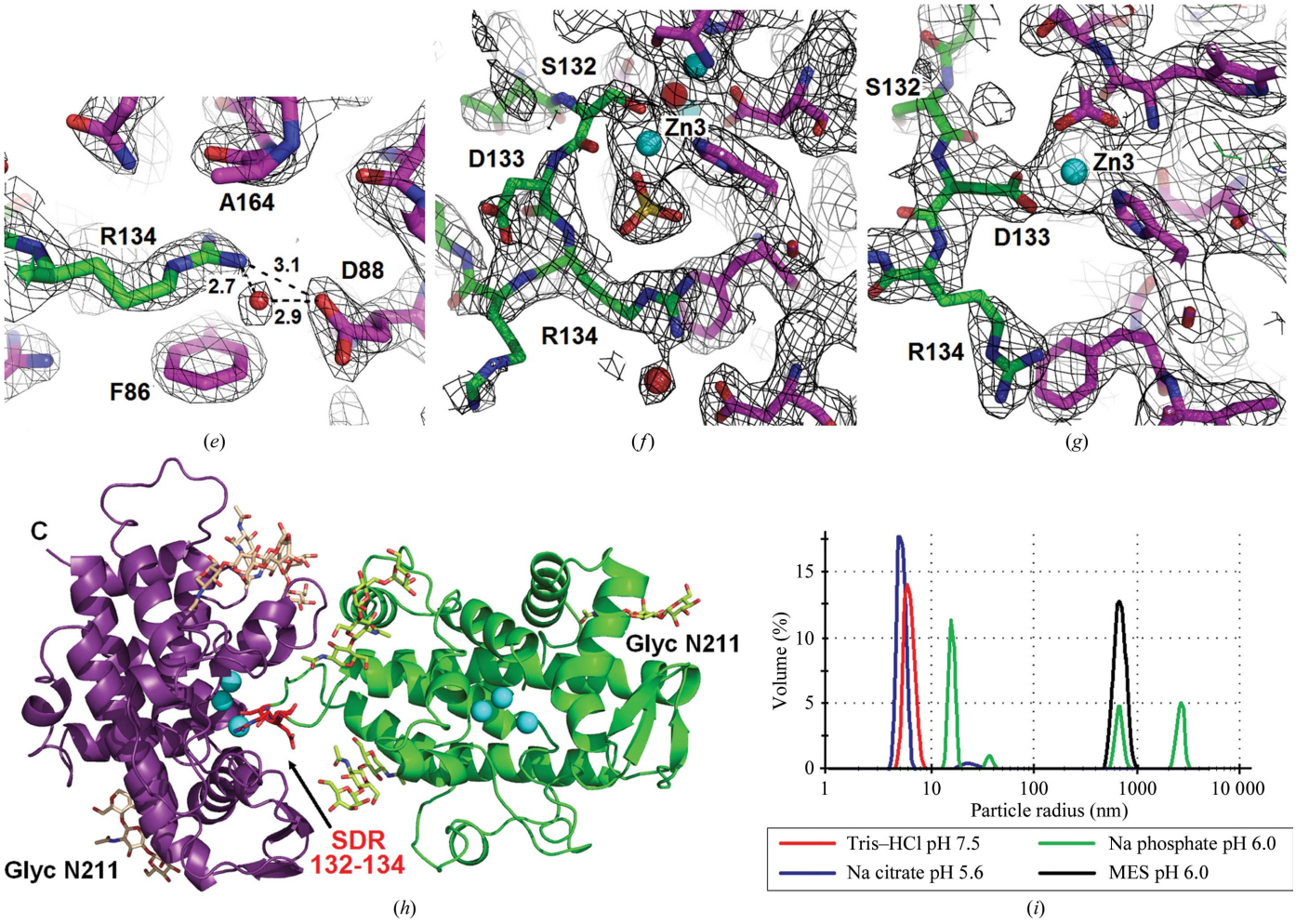

Figure 2 (continued)
(*e*) Binding of Arg134 of R-TBN1wt (green) to the nucleobase pocket of a neighbouring molecule of R-TBN1wt (magenta). Distances are given in Å. (*f*) Binding of the SDR loop of R-TBN1wt (green) into the active site of a neighbouring molecule of R-TBN1wt (magenta). (*g*) Binding of the SDR loop of R-TBN1-N211D (green) into the active site of the neighbouring molecule (magenta). (*h*) Dimer of TBN1 involved in oligomerization. The molecule providing the SDR loop is shown in green, with pale green oligosaccharides. The molecule accepting the loop in the active site is shown in purple, with light yellow oligosaccharides. Zn^{2+} ions are shown as pale blue spheres and the side chains of the SDR loop are shown as red sticks. (*i*) The effect of buffer on the oligomerization state of R-TBN1wt shown as particle-size distributions by their volume measured by DLS. The buffers were titrated close to the optimal pH for TBN1 activity. All molecular graphics were created using *PyMOL* (DeLano, 2004). The $2F_o - F_c$ map is contoured at the 1σ level in all cases.

W703 completes the coordination for distorted octahedral geometry of Zn2 with a relatively long contact distance of 2.5 Å. In both molecules of R-TBN1-N211D a Cl^- ion is bound in the same position as in R-TBN1wt. A positively charged ion is bound on the surface of R-TBN1-N211D, making five coordination bonds to Arg100 O, His103 N^{ε} and three water molecules. Only sodium and magnesium ions were present in the mother solution at significant concentrations. The concentration of sodium ions was approximately twice that of magnesium ions and the ion showed relatively irregular coordination and long contact distances. Therefore, a sodium ion was modelled in chain *B*. Disorder in this area in chain *A* prevented clear interpretation of the electron density and although the presence of sodium is probable, only waters were modelled. The last 11 and 12 amino acids of the C-termini in chains *A* and *B*, respectively, were not localized in electron density and were not built.

The different space group and content of the asymmetric unit in the case of R-TBN1-N211D in comparison with R-TBN1wt are a result of changes in intermolecular interactions caused by the mutation. The missing oligosaccharide chain enables the formation of interactions to the residues in this area and leads to different packing in the corresponding surface region.

3.4. TBN1 oligomerization

Both R-TBN1wt and R-TBN1-N211D are present in the form of monomers and asymmetric dimers in the storage buffer (Supplementary Fig. S1[1]). A fine equilibrium between these two states can easily be shifted and the formation of

[1] Supplementary material has been deposited in the IUCr electronic archive (Reference: WD5194). Services for accessing this material are described at the back of the journal.

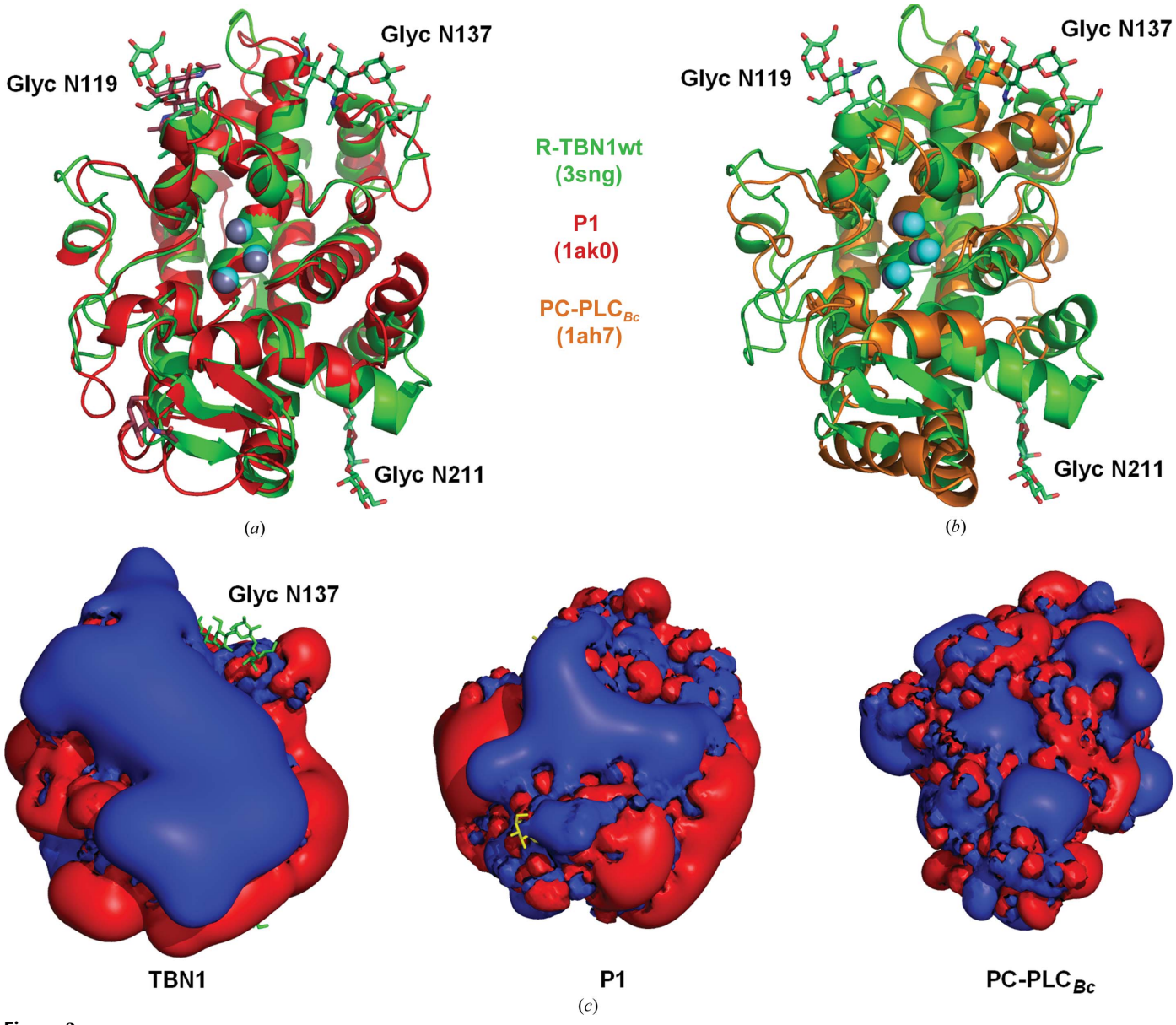

Figure 3
(*a*) Superposition of the structures of P1 nuclease (PDB entry 1ak0; Romier *et al.*, 1998; red) and R-TBN1wt (PDB entry 3sng; green). Glycans are displayed as sticks and Zn^{2+} ions in the centre of the active site are shown as pale blue (TBN1) and grey (P1) spheres. (*b*) Superposition of the structures of PC-PLC$_{Bc}$ (PDB entry 1ah7; Hough *et al.*, 1989; orange) and R-TBN1wt (PDB entry 3sng; green). Zn^{2+} ions in the centre of the active site are shown as grey (PC-PLC$_{Bc}$) and pale blue (TBN1) spheres. (*c*) Isosurface of electrostatic potential at pH 6 (contoured at levels of 1 *kT*/*e*, blue, and −1 *kT*/*e*, red) of TBN1, P1 nuclease and PC-PLC$_{Bc}$ in the same orientation as in (*a*) and (*b*). Notice the continuous positive face of TBN1 ready for double-stranded substrate binding.

higher oligomers can also be elicited by changing the composition of the solution. The effects of buffers on the oligomerization state of R-TBN1wt were monitored by DLS (Fig. 2*i*) at a pH close to the optimum for nuclease activity of TBN1. 2-(*N*-Morpholino)-ethanesulfonic acid (MES) causes almost complete aggregation of R-TBN1wt. NaH_2PO_4/Na_2HPO_4 buffer leads to oligomerization and aggregation of TBN1. Sodium citrate buffer has no effect in comparison with the original storage buffer.

The leading interaction which drives oligomerization in solution and also crystallization is most likely to be the intermolecular interaction of the SDR loop, as described above. The assembly of monomers into dimers is close to identical in R-TBN1wt and R-TBN1-N211D. In the wild-type structure the second molecule of the dimer is generated by the symmetry operator $-y-1, x-y, z+1/3$ or $-x+y-1, -x-1, z-1/3$. In the case of the N211D mutant, the dimer forms the asymmetric unit. The buried area of the dimer interface calculated for the R-TBN1wt structure by the *PISA* server (Krissinel, 2010) is 759 Å^2, which is 5.9% of the solvent-accessible surface. The asymmetric dimer is shown in Fig. 2(*h*).

3.5. Glycosylation

Attempts to produce TBN1 in *E. coli* led to insoluble protein (data not shown). Deglycosylation of R-TBN1wt using PNGase F leads to the formation of aggregates (Supplemen-

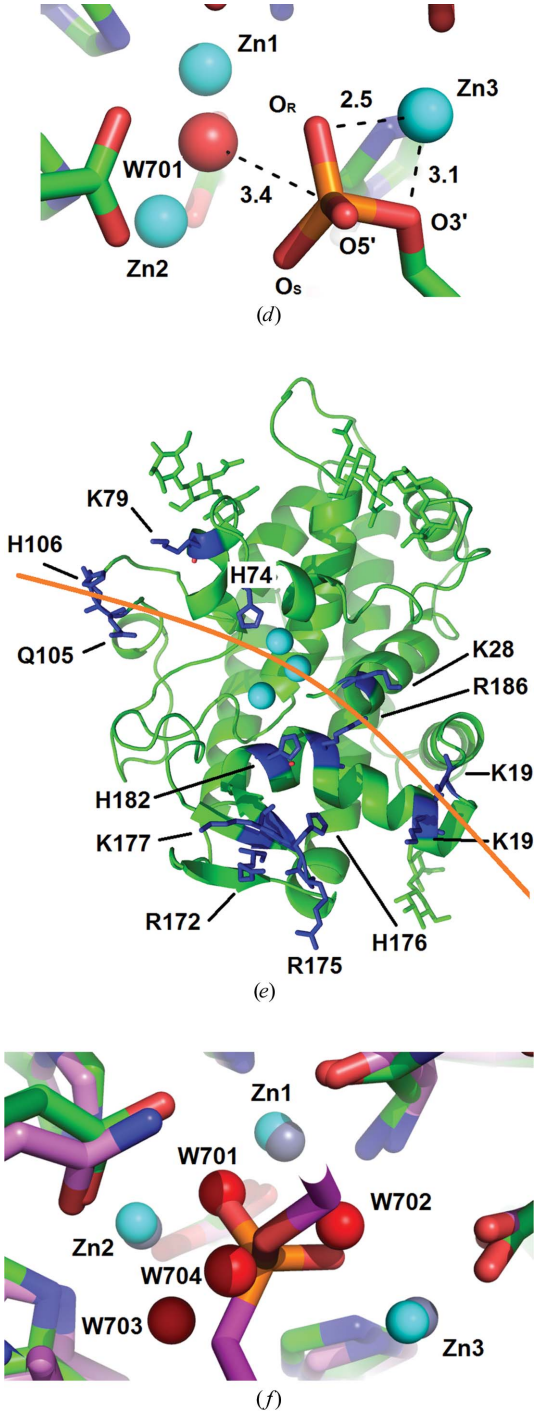

Figure 3 (continued)
(*d*) The position of 3′-AMP resulting from docking of the ligand into the active site of TBN1. The phosphate group is bound to the Zn^{2+} cluster in a manner that confirms the proposed reaction mechanism. (*e*) Residues around the active-site groove of TBN1 proposed to be involved in dsDNA binding, represented as blue sticks. The proposed binding direction of dsDNA is shown as an orange line. (*f*) The superposition of the active sites of R-TBN1-N211D (PDB entry 4dj4) and of the PC-PLC$_{Bc}$ complex with substrate analogue (PDB entry 1p6d; Antikainen *et al.*, 2003) suggests a possible binding mode of the phosphate group of the phospholipid substrates (magenta) into the active site of TBN1. Four water molecules present in the active site of TBN1 (W701–W704) must be displaced upon binding. The graphics were created using *PyMOL* (DeLano, 2004).

tary Fig. S2). The reason for this behaviour lies in the fact that oligosaccharides shield the hydrophobic areas on the surface of the protein. The oligosaccharide bonded to Asn119 forms hydrogen bonds to Gln123, is involved in a direct stacking interaction with Trp80 and shields Phe120 and also Phe144 partially. The total surface area shielded by this oligosaccharide (calculated for the R-TBN1wt structure using *PISA*; Krissinel, 2010) is 388 Å^2. The Asn137 oligosaccharide forms hydrogen bonds to Tyr57 and Glu140. It shields Leu65, Trp68, Leu143 and also Pro55 partially. The total surface area shielded by this oligosaccharide is 296 Å^2. The Asn211 oligosaccharide partially shields a hydrophobic pocket composed of Leu204, Ile208, Leu268 and Met272. The total surface area shielded by this oligosaccharide is 266 Å^2. The localized parts of glycans together cover about 950 Å^2 of the enzyme surface, *i.e.* 7.5% of the solvent-accessible surface.

3.6. Activity of TBN1 with methylated lysine residues

The importance of lysine residues in the reaction mechanism was investigated by a comparison of the activity between native R-TBN1wt and R-TBN1wt with methylated lysine residues. In all three substrate cases (RNA, ssDNA and dsDNA), a measurable decrease of specific activity in comparison with unmodified R-TBN1wt occurred (62 ± 2, 85 ± 3 and 58 ± 5%, respectively; experimental errors were determined from three independent measurements). The strongest effect was measured for dsDNA and the weakest effect was measured for ssDNA.

3.7. Phospholipase activity

The average specific phospholipase activity of R-TBN1wt with *p*-NPPC at pH 7.3 and 310 K is 12 pmol min^{-1} µg^{-1} under the given reaction conditions. The phospholipase activity of R-TBN1wt was confirmed by a second experiment designed to exclude the possibility that the phospholipase activity of the sample is caused by the residual presence of phosholipase C or enzymes with similar activity. The composition of the reaction solution was similar to that in the first experiment but differently treated rhombohedral crystals of R-TBN1wt were used as enzyme samples. Owing to crystal packing, the active sites of the enzyme molecules in these crystals are not accessible. Therefore, the expected activity of undissolved crystals would be minimal to zero. Crystals were collected from a crystallization drop and washed several times in the enzyme-storage buffer. Four types of samples were prepared: (i) crystals crushed in the storage buffer but not dissolved, (ii) crystals crushed, not dissolved and treated with EDTA, (iii) crystals dissolved in the storage buffer with the addition of NDSB-201 and (iv) crystals dissolved as in (iii) and treated with EDTA. The measured absorbance of released *p*-nitrophenol at λ = 660 nm with regard to background was 0.158 after 5 d of reaction in the dark at 298 K. Only the sample prepared from the crystals dissolved and not treated with EDTA (sample type iii) showed activity against *p*-NPPC.

As a second, independent assay, cleavage of L-α-phosphatidylcholine (PC), a native substrate of phosphatidylcholine-

preferring phospholipase C from *Bacillus cereus* (PC-PLC$_{Bc}$), was also confirmed. As in the above experiments, TBN1 had already been confirmed as the catalyst responsible for this type of activity; the native sample of R-TBN1wt in solution was only used in the second assay. Two independent measurements were performed and the released phosphate ions were detected by colorimetric analysis using the Ames Colour Reagent (Barrows *et al.*, 1985). The measured absorbance at λ = 660 nm with regard to background was 0.125 $\pm$ 0.008.

4. Discussion

The structure of TBN1 was solved using two different crystal forms. The best data collected from the first (rhombohedral) form had a resolution limit of 3.2 Å, but the diffraction was anisotropic with strong diffuse scattering. Despite the low quality of the data, it was possible to solve the phase problem using only two-wavelength MAD and to build a preliminary model of the structure using MR and the initial phases from the MAD solution (Koval' *et al.*, 2011). However, this crude model could only be improved and refined after the second (trigonal) form of the TBN1 crystals was obtained a year later. The described complexity of the structure-solution process has its roots in the behaviour of TBN1 molecules (oligomerization and rich surface glycosylation) and the related fast growth of the crystals in only one direction.

TBN1 has a phospholipase C-like/P1 nuclease fold and contains three catalytic metal ions in a cluster identified by X-ray fluorescence as zinc (Koval' *et al.*, 2011). Its tertiary structure is stabilized by four disulfide bridges, which was observed for the first time in this type of enzyme. The active site is localized at the bottom of a wide groove, which together with its surroundings forms a large positively charged face at the surface of TBN1. The position of the active site is clear from the presence of the zinc ions and the metal-dependent activity of TBN1 (Podzimek *et al.*, 2011) and also from comparison with the structure of P1 nuclease (see below). The active site is capable of binding nucleic acids, phospholipids and also peptide chains, which makes TBN1 one of the most promiscuous nucleases known. Homologous enzymes from *Humulus lupulus* (HBN1; UniProt sequence accession code B4ERM5; Matousek *et al.*, 2008) and from *Arabis brassica* (ABN1; UniProt sequence accession code E3PQH5; Podzimek *et al.*, 2011), with 79 and 72% sequence identity to TBN1, preserve all of the described features at the sequence level and therefore these properties are common to HBN1, ABN1 and likely to all members of plant nuclease I family homologous to TBN1.

4.1. Comparison with P1 nuclease

The closest related nuclease with known structure is P1 nuclease from *Penicillium citrinum* (Volbeda *et al.*, 1991; Romier *et al.*, 1998), with 31% sequence identity (for a structure-based sequence alignment of TBN1 and P1, see Supplementary Fig. S3). Both enzymes are Zn^{2+}-dependent with an acidic pH optimum. The main difference between TBN1 and P1 lies in the fact that TBN1 also efficiently cleaves dsDNA and other highly organized nucleic acids, whereas P1 shows only negligible activity towards these substrates. A superposition of TBN1 with P1 (PDB entry 1ak0; Romier *et al.*, 1998) calculated using *PDBeFold* (Krissinel & Henrick, 2004) resulted in a positional r.m.s.d. of 1.56 Å between their C$^{\alpha}$ atoms (242 residues aligned). The fold is similar in both structures (Fig. 3*a*) and they have a similar arrangement of the catalytic Zn^{2+}-ion cluster together with the zinc-coordinating residues. The fold of P1 nuclease is stabilized by two disulfide bridges. These disulfide bridges are also present in TBN1 (SS2 and SS3; Fig. 1). TBN1 contains two additional disulfide bridges (SS1 and SS4; Fig. 1). P1 contains four N-glycosylation sites, while TBN1 only contains three; Asn119 (TBN1 numbering) is the only site that is conserved. The Phe-site is present with a similar composition in both enzymes with only a minor change: Ala164 is substituted by Val in P1 with no effect on the Phe-site shape and thus function. P1 contains a second nucleobase site: the Tyr-site (Romier *et al.*, 1998). It is not conserved in TBN1, and no other possible nucleobase-binding site was identified in TBN1. Important differences between TBN1 and P1 are found in the overall shape and electrostatic potential distribution (Figs. 3*a* and 3*c*) of the active-site grooves. These are most likely to be responsible for the differences between the activity of TBN1 and P1 towards structured nucleic acids (discussed below).

4.2. Comparison with PC-PLC$_{Bc}$

Phosphatidylcholine-preferring phospholipase C from *B. cereus* (PC-PLC$_{Bc}$) is a small bacterial Zn^{2+}-dependent phosphodiesterase that is capable of the cleavage of various phospholipids, producing diacylglycerol (DAG) and a corresponding alkyl phosphate as end products (Hansen *et al.*, 1993). PC-PLC$_{Bc}$ (PDB entry 1ah7; Hough *et al.*, 1989) is the second most similar enzyme to TBN1 with known structure. The positional r.m.s.d. for C$^{\alpha}$ atoms (176 residues aligned) is 2.61 Å (*PDBeFold*; Krissinel & Henrick, 2004). Despite a very low sequence identity between TBN1 and PC-PLC$_{Bc}$ (16% calculated using the superimposed chains; a structure-based sequence alignment of TBN1 and PC-PLC$_{Bc}$ is shown in Supplementary Fig. S4), the enzymes share a similar fold (Fig. 3*b*) and have an almost identical arrangement of the catalytic Zn^{2+} cluster; almost all of the coordination residues are also identical. There is no active-site cleft in the case of PC-PLC$_{Bc}$; instead, the catalytic Zn^{2+} cluster is located at the bottom of a cavern composed of residues involved in binding and proper orientation of substrate for hydrolysis (Benfield *et al.*, 2007). TBN1 offers a more open site to enable the cleavage of the 'backbone' of very large nucleic acids. Although TBN1 and PC-PLC$_{Bc}$ have a similar fold, the overall shape of the molecules and also their surface electrostatic potential distributions are entirely different (Fig. 3*c*).

4.3. Role of glycosylation

The main role of glycosylation in TBN1 is the enhancement of stability and solubility. This was proven by two separate

experimental results: the unsuccessful attempts to express TBN1 in *E. coli*, which led to insoluble protein, and the deglycosylation experiments, which led to aggregation. The reason for this behaviour lies in the fact that the three oligosaccharides shield large hydrophobic areas on the surface of TBN1 (7.5% of the surface). Exposure of these areas can lead to hydrophobicity-driven aggregation as well as to protein misfolding. It should also be noted that the oligosaccharides on Asn199 and Asn137 also participate in oligomerization by interactions with the peptide chain of a neighbouring molecule, even if with only a minor contribution to the dimer-forming interactions.

4.4. Role of oligomerization

The oligomerization of TBN1 is strongly affected by the composition and parameters of the solution such as pH, temperature or ionic strength as well as by the concentration of TBN1 itself. The results of size-exclusion chromatography of native R-TBN1wt and native R-TBN1wt treated with EDTA confirm the formation of dimers in solution, as well as the possibility of shifting the balance between dimers and monomers. DLS of R-TBN1wt in alternative buffers shows varied formation of oligomers and aggregates in the presence of phosphate anions. Each crystal form of TBN1 observed to date (including unpublished results) always relies on the main lattice-forming interaction: the binding of the SDR loop into the active site of another molecule. Therefore, we conclude that this is also the leading interaction causing oligomerization in solution. It is expected that phosphate anions can bind in the active site of TBN1 in a similar fashion as sulfate anions (in the case of the R-TBN1wt structure; Fig. 2*f*) and enhance the binding of the SDR loop from the neighbouring molecule by stabilizing the position and contact of Arg134 (Fig. 2*f*). In this way, phosphate ions can enhance oligomerization. Such a tight interaction of a peptide with a nuclease active site has not been observed to date, as well as the formation of asymmetric dimers with a strong dependence on the environment. We propose that these interactions play a role in regulation of the activity of TBN1. Phosphate anions are naturally present in all living cells and can also be produced by the cleavage of 3′-nucleotides by TBN1. The presence of active TBN1 in a cell leads to apoptotic processes; therefore, expression of TBN1 in plant cells must be a strictly regulated process. Moreover, it has been described that several ribonucleases along with the bifunctional nuclease I are induced by phosphate starvation (Chen *et al.*, 2000), suggesting a regulatory role of phosphate in nuclease activation. This activation could include RNA expression level as well as regulation of oligomerization by P_i levels. However, oligomerization of TBN1 *in vivo* has not yet been investigated.

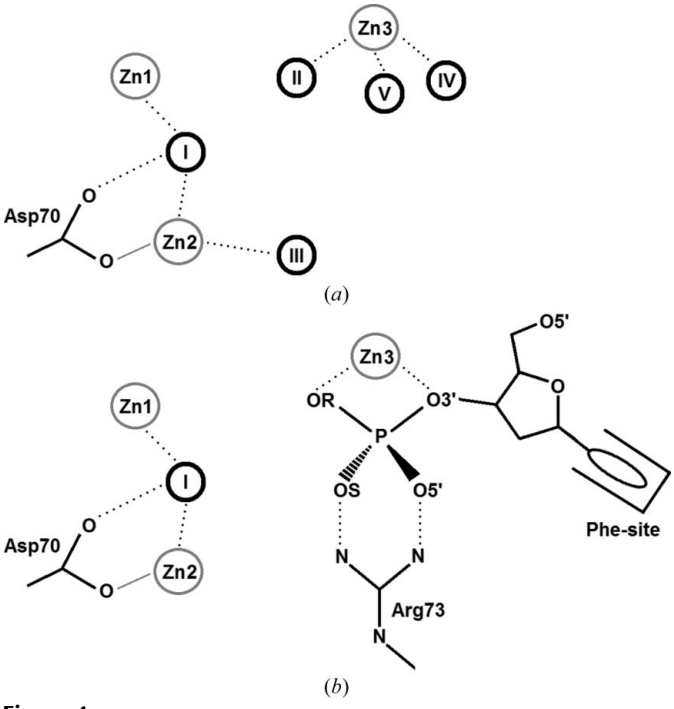

Figure 4
Schematic representation of the binding positions available for O atoms in the first coordination sphere of the catalytic zinc cluster. (*a*) The TBN1 active site without a ligand. All five binding positions (circles designated by I–V; the labelling corresponds to the positions W701, W702, W703, SO_4^{2-} O^1 and Ser132 O, respectively) are occupied by water. (*b*) Substrate binding to the active site. The nucleobase binds into the Phe-site; the scissile phosphate binds to the zinc ion, replacing the waters in positions II and IV by OR and O3′, and displacing waters from positions III and V. The water in position I is activated and serves as the nucleophile. Binding of the phosphate group is stabilized by Arg73.

4.5. Ligand binding to the active site of TBN1

Productive binding of a nucleic acid or a 3′-mononucleotide to the active site consists of binding of the nucleobase (at the 5′ end of the nucleotide with respect to the cleaved bond) into the Phe-site and binding of the scissile phosphate to the zinc cluster. The Phe-site is formed by Phe86 and Ala164 (providing stacking interactions with the aromatic ring of a bound base) and by Asp88 at the end of the pocket (hydrogen bonding). Following from the analysis of the present structures, there are five positions available for binding of oxygen in the first coordination sphere of the zinc ions (Fig. 2*c*). One water molecule (hydroxide ion) W701 (I) bridges Zn1 and Zn2 and also forms a hydrogen bond to Asp70 in each active-site structure. Water in this position is likely to be activated and plays the role of a nucleophile in the reaction mechanism. The position W702 (II) is occupied by water in two cases and by the O atom of the SDR loop/ligand (Ser132 O^{γ}) in one case. Therefore, this water site represents a possible ligand-binding site. The second ligand-binding site is the position of SO_4^{2-} O^1 or Asp133 $O^{\delta2}$ (IV) of the SDR loop. The exact position for oxygen binding in this case is less conserved in comparison with the W702 position as it is more exposed to solvent. Position W703 (III) is occupied by water only in the R-TBN1-N211D structure. In this case, Arg73 is free from ligands and is in a conformation that allows solvent access to Zn2. The position W703 is vacant in the R-TBN1wt structure. In this case Arg73 binds the ligand (SO_4^{2-}) and is in a conformation which spatially forbids occupation of the W703 site. The

position of Ser132 O (V) is only occupied in the case of the R-TBN1wt structure with a long coordination distance (2.6 Å) and is the least conserved position. All of the binding positions are shown in Fig. 2(*c*) and schematically in Fig. 4(*a*).

Between the zinc cluster and the Phe-site, there are two residues that are likely to be involved in the reaction mechanism: Arg73 and Asn167 (Fig. 2*d*). The side chain of Arg73 is placed between Zn2 (Arg73 $N^{\eta1}$ is 4.1 Å from Zn2 in R-TBN1wt) and Phe86 and can adopt several conformations as follows from the comparison of the TBN1 wild-type and N211D mutant structures. Asn167 is conserved in P1 and also in PC-PLC$_{Bc}$; therefore, it is expected to play a certain role in the active site. The side chain of Asn167 is stabilized between Zn3 and Ala164, to which it forms a hydrogen bond. This interaction not only stabilizes Asn167 in its position but also helps to properly stabilize and shape the Phe-site. In the case of PC-PLC$_{Bc}$, Asn167 serves as a binding partner for the diacylglycerol group (Hansen *et al.*, 1993). In the structure of the complex of P1 nuclease with a substrate analogue, Asn167 forms a hydrogen bond to the ribose moiety of the ligand (Romier *et al.*, 1998). From these findings and our results from docking calculations, it follows that the second H atom present on Asn167 $N^{\delta2}$ is capable of forming another hydrogen bond oriented towards the predicted position of the bound ribose (deoxyribose) moiety of a substrate. Based on these observations, we postulate that Asn167 plays an important role in the proper formation of the active site, especially of the Phe-site, and also in substrate binding.

4.6. Proposed mechanism of P—O3′ bond cleavage

On the basis of this analysis of the potential binding positions near the metal cluster we suggest the following mechanism, which is in agreement with the proposed reaction mechanism for P1 nuclease (Romier *et al.*, 1998) and is also supported by our results from the docking of adenosine 3′-monophosphate (3′-AMP) into the active site of TBN1. In the presence of the 'activated' water molecule W701, the placement of the adenine base into the Phe-site enables the positioning of the scissile phosphate so that the P—O3′ bond lies almost in line with W701 at a distance suitable for nucleophilic attack (Fig. 3*d*). O3′ and OR of the phosphate group of a substrate bind to Zn3, displacing two water molecules from the positions of SO_4^{2-} O^1 and W702, respectively, and possibly also water from the position of Ser132 O (Fig. 3*d*). O5′ and OS form bonds to the guanidinium group of Arg73, which results in the release of W703. The phosphate group in this configuration is prepared for nucleophilic attack by water W701, previously activated by Zn1 and Zn2. The proposed binding of a substrate into the active site is schematically shown in Fig. 4(*b*). Asp70 is important for proper orientation of W701 before the attack. Hydrolysis of the P—O3′ bond is then carried out by a nucleophilic in-line attack of the activated water molecule (hydroxide ion) on the scissile phosphate with inversion of configuration at the P atom (Volbeda *et al.*, 1991). A reaction intermediate with the P atom coordinated by five O atoms is stabilized by Arg73. The transition state is then decomposed by breakage of the P—O3′ bond. The leaving 3′-hydroxyl group is stabilized by Zn3. The release of the products is accompanied by entropy-driven binding of water molecules to the active site (positions I–V), which also provides the new water to be activated for the next cycle (position I).

4.7. Proposed mechanism for binding and cleavage of dsDNA and other structured nucleic acids

TBN1 is capable of cleavage of DNA and RNA with almost any secondary structure, including highly stable viroid RNA (Podzimek *et al.*, 2011). As described previously, the most probable catalytic mechanism of P—O3′ bond cleavage involves binding of the −1 base with respect to the cleaved bond into the Phe-site. In order to do so in the case of nucleic acids with secondary structure, such as B-form dsDNA, the secondary structure must be deformed and the nucleic acid partially unwound. The Phe-site itself can assist in DNA unwinding, as suggested previously for the Klenow fragment (Freemont *et al.*, 1988), which possesses a similar nucleobase-binding site. Nevertheless, it is clear from the structural comparison with P1 nuclease that the presence of the nucleobase-binding site alone is not sufficient for the successful cleavage of dsDNA, which must be first stabilized in the proper position and orientation across the active site. The trinuclear catalytic cluster is surrounded by a large positive face composed of the positively charged groove along with surrounding positive patches (Fig. 3*e*). This positive face is not conserved in the related P1 nuclease, and P1 is not capable of effective dsDNA cleavage. Docking of dsDNA to TBN1 suggests the role of this positive face as the binding surface for dsDNA and also very likely other nucleic acids with secondary structure. Currently, there is no experimental information about the residues that interact with dsDNA upon its binding to TBN1, but from the structural data, surface electrostatic potential distribution, docking and lysine-methylation experiments we can assume the importance of several sites (Fig. 3*e*). The first site is a finger-like Gln105/His106 site at one end of the active-site groove, which is at a distance of 15–20 Å from Zn3. The second site is the Lys28/Arg186 site, which is at a distance of 12–15 Å from Zn3. The third site is the Lys194/Lys199 site. The Lys28/Arg186 and Lys194/Lys199 sites are approximately 12 Å apart, which corresponds to the width of the minor groove of the B-form of dsDNA. The fourth site is a positive patch composed of Arg172, Arg175, His176 and Lys177 located on the only β-sheet present in TBN1. There are also three other positive residues in the active-site groove with a possible role in substrate binding: His74, Lys79 and His182. The mentioned residues, except for Lys79, which is substituted by Arg in both cases, are conserved in TBN1 homologues from *H. lupulus* (HBN1) and from *A. brassica* (ABN1).

The importance of Lys residues in TBN1 was experimentally confirmed by an activity comparison between native R-TBN1wt and a sample with methylated lysine residues. Methylation leads to a decrease in TBN1 activity towards all substrates (RNA, ssDNA and dsDNA), with the most signif-

icant decrease recorded for dsDNA cleavage. The state of the enzyme after methylation was checked by DLS and the particle-size distribution was similar to that of the native sample. Consequently, the change in activity is not caused by aggregation or denaturation of TBN1 after or during methylation and must be linked to the changes at the Lys residues. Decreased activity towards all substrates could indicate that Lys residues are involved in binding of all longer substrates, not only dsDNA. On the other hand, the activity was not completely abolished but rather significantly decreased. This could be caused by incomplete methylation of the sample and also by the fact that other residues beside lysines (presumably the arginines and histidines mentioned above) are also involved in the binding of large substrates.

4.8. Phospholipase activity

The phospholipase C-like activity results in release of diacylglycerol (DAG). DAG is an important second messenger which can activate intracellular phosphorylation cascades and is involved in many crucial cell life-cycle processes, including triggering of apoptosis and senescence, in plants (Borochov *et al.*, 1995). TBN1 itself is an enzyme that is tightly connected to apoptosis in plants (Matousek *et al.*, 2007) and its phospholipase C-like activity has been confirmed *in vitro*. In the light of these facts and our experimental results, we hypothesize that DAG release could be one of the mechanisms of action of TBN1 in the case of apoptosis and cellular senescence processes.

The binding mode of phospholipids to the active site of TBN1 is not yet known; however, the environment directly surrounding the catalytic Zn^{2+} cluster offers several possibilities. From the superposition of the structures of TBN1 and PC-PLC$_{Bc}$ in complex with a substrate analogue [(3*S*)-3,4-di-*N*-hexanoyloxybutyl-1-phosphocholine; PDB entry 1p6d; Antikainen *et al.*, 2003] it is clear that there are no steric clashes that prevent the interaction of such a phospholipid with the TBN1 active site and that the formation of such a complex is possible in a similar way. In the active site of PC-PLC$_{Bc}$ the diacylglycerol moiety is bound by two hydrogen bonds. The *sn*-1 carbonyl O atom is part of the hydrogen-bonding network and the *sn*-2 carbonyl O atom forms a hydrogen bond to Asn134 N$^{\delta2}$. Interestingly, Asn134 is conserved in TBN1 as Asn167 and both interactions of the carbonyl O atoms are also possible in TBN1. Binding of the phosphate group within the Zn^{2+} cluster in the manner observed in PC-PLC$_{Bc}$ would result in the displacement of water molecules W701–W704 from the active site, as observed in PC-PLC$_{Bc}$ (Antikainen *et al.*, 2003; Fig. 3*f*). Therefore, W701, which serves as a nucleophile for the nuclease activity, would be missing and the observed phospholipase C-like catalysis of TBN1 would be likely to rely on another nucleophile.

4.9. Consequences for possible anticancer therapy

A number of ribonucleases from animals and fungi capable of inhibition of tumour growth have been found (Matousek, 2001). Among the most potent are onconase (ONC) isolated from oocytes and embryos of *Rana pipiens* (Darzynkiewicz *et al.*, 1988; Ardelt *et al.*, 1991) and α-sarcin from *Aspergillus giganteus* (Olson & Goerner, 1965). Anticarcinogenic effects of nucleases from the plant nuclease I family have also recently been demonstrated. These include mung bean sprout nuclease (Soucek *et al.*, 2006), extracellular nuclease from black pine pollen (Lipovova *et al.*, 2008), recombinant HBN1 nuclease from *H. lupulus* and also recombinant TBN1 nuclease, which has successfully been tested against human tumours *in vivo* (Matousek *et al.*, 2009, 2010).

Several of the findings presented above can be utilized in order to enhance the potential of TBN1. The newly discovered multifunctionality of TBN1 significantly broadens its possible role in living systems and suggests that, aside from the decomposition of nucleic acids and 3′-nucleotides, TBN1 can probably interfere with intracellular signalling pathways. Oligomerization of TBN1 occludes those active sites which are involved in the interactions and changes the overall shape and surface properties of the enzyme. Therefore, oligomerization will have effects on the specific activity levels depending on the substrate size and type.

5. Conclusions

TBN1 possesses the phospholipase C-like/P1 nuclease fold stabilized by four disulfide bridges and its three N-linked oligosaccharides shield hydrophobic areas totalling 7.5% of the molecular surface. The active site is localized at the bottom of the central positively charged groove and contains three Zn^{2+} ions essential for enzymatic activity. TBN1 can oligomerize and is present in the form of asymmetric dimers and monomers in solution in a controllable equilibrium. A key factor in oligomerization is the binding of the SDR loop (132–134) of TBN1 into the active site of another molecule. This oligomerization effect could be part of the regulation of TBN1 activity in plant cells after expression and maturation.

The reaction mechanism of the phosphoesterase activity involves hydrolysis of the P—O3′ bond of a substrate by in-line attack of an activated water molecule (hydroxide ion) on the scissile phosphate with inversion of configuration at the P atom. The water molecule is activated by the Zn1–Zn2 pair and properly orientated by Asp70.

We propose that stabilization and proper binding of dsRNA and DNA and nucleic acids with secondary structure is secured by the large positively charged face on the enzyme surface involving five lysine, three arginine and four histidine residues localized in the positive patches around the active-site groove. The methylation of lysine residues decreases specific activity preferentially on double-stranded substrates.

The phospholipase activity of TBN1 was detected and confirmed for the first time. TBN1 can thus be classified as a multifunctional enzyme capable not only of the hydrolysis of nucleic acids and mononucleotides but also of the cleavage of phospholipids. All of these activities could be responsible for its observed *in vivo* effects, namely in plant senescence and in tumour-growth inhibition.

This project was supported by the Czech Science Foundation, projects P302/11/0855, 310/09/1407, 202/06/0757 and 521/09/1214, and by the EC under ELISA grant agreement No. 226716 (synchrotron-access funding, projects 09.2.90262 and 10.1.91347). In addition, the work was supported by RVO: 60077344. We also gratefully acknowledge support from Praemium Academiae of AS CR and from the Ministry of Education, Youth and Sports of the Czech Republic (grant No. CZ.1.07/2.3.00/30.0029). The authors wish to thank Dr N. Darowski and Dr U. Müller of the Helmholtz-Zentrum Berlin for support at beamline BL14.1 of BESSY II.

References

Antikainen, N. M., Monzingo, A. F., Franklin, C. L., Robertus, J. D. & Martin, S. F. (2003). *Arch. Biochem. Biophys.* **417**, 81–86.
Ardelt, W., Mikulski, S. M. & Shogen, K. (1991). *J. Biol. Chem.* **266**, 245–251.
Baker, N. A., Sept, D., Joseph, S., Holst, M. J. & McCammon, J. A. (2001). *Proc. Natl Acad. Sci. USA*, **98**, 10037–10041.
Banitt, I. & Wolfson, H. J. (2011). *Nucleic Acids Res.* **39**, e135.
Barrows, J. N., Jameson, G. B. & Pope, M. T. (1985). *J. Am. Chem. Soc.* **107**, 1771–1773.
Benfield, A. P., Goodey, N. M., Phillips, L. T. & Martin, S. F. (2007). *Arch. Biochem. Biophys.* **460**, 41–47.
Borochov, A., Spiegelstein, H. & Porat, R. (1995). *Acta Hortic.* **405**, 240–245.
Chen, V. B., Arendall, W. B., Headd, J. J., Keedy, D. A., Immormino, R. M., Kapral, G. J., Murray, L. W., Richardson, J. S. & Richardson, D. C. (2010). *Acta Cryst.* D**66**, 12–21.
Chen, D. L., Delatorre, C. A., Bakker, A. & Abel, S. (2000). *Planta*, **211**, 13–22.
Darzynkiewicz, Z., Carter, S. P., Mikulski, S. M., Ardelt, W. J. & Shogen, K. (1988). *Cell Tissue Kinet.* **21**, 169–182.
DeLano, W. L. (2004). *Abstr. Pap. Am. Chem. Soc.* **228**, 030-CED.
Dohnálek, J., Koval', T., Lipovová, P., Podzimek, T. & Matoušek, J. (2011). *J. Synchrotron Rad.* **18**, 29–30.
Dolinsky, T. J., Nielsen, J. E., McCammon, J. A. & Baker, N. A. (2004). *Nucleic Acids Res.* **32**, W665–W667.
Emsley, P. & Cowtan, K. (2004). *Acta Cryst.* D**60**, 2126–2132.
Freemont, P. S., Friedman, J. M., Beese, L. S., Sanderson, M. R. & Steitz, T. A. (1988). *Proc. Natl Acad. Sci. USA*, **85**, 8924–8928.
Gouet, P., Courcelle, E., Stuart, D. I. & Métoz, F. (1999). *Bioinformatics*, **15**, 305-308.
Hansen, S., Hough, E., Svensson, L. A., Wong, Y.-L. & Martin, S. F. (1993). *J. Mol. Biol.* **234**, 179–187.
Hough, E., Hansen, L. K., Birknes, B., Jynge, K., Hansen, S., Hordvik, A., Little, C., Dodson, E. & Derewenda, Z. (1989). *Nature (London)*, **338**, 357–360.
Kim, Y. *et al.* (2008). *Nature Methods*, **5**, 853–854.
Koval', T., Lipovová, P., Podzimek, T., Matoušek, J., Dušková, J., Skálová, T., Štěpánková, A., Hašek, J. & Dohnálek, J. (2011). *Acta Cryst.* F**67**, 124–128.
Krissinel, E. (2010). *J. Comput. Chem.* **31**, 133–143.
Krissinel, E. & Henrick, K. (2004). *Acta Cryst.* D**60**, 2256–2268.
Kurioka, S. & Liu, P. V. (1967). *Appl. Environ. Microbiol.* **15**, 551555.
Kurioka, S. & Matsuda, M. (1976). *Anal. Biochem.* **75**, 281–289.
Li, H., Robertson, A. D. & Jensen, J. H. (2005). *Proteins*, **61**, 704–721.
Lipovova, P., Podzimek, T., Orctova, L., Matousek, J., Pouckova, P., Soucek, J. & Matousek, J. (2008). *Neoplasma*, **55**, 158–164.
Matousek, J. (2001). *Comp. Biochem. Physiol. C Toxicol. Pharmacol.* **129**, 175–191.
Matousek, J., Kozlová, P., Orctová, L., Schmitz, A., Pesina, K., Bannach, O., Diermann, N., Steger, G. & Riesner, D. (2007). *Biol. Chem.* **388**, 1–13.
Matousek, J., Orctová, L., Skopek, J., Pesina, K. & Steger, G. (2008). *Biol. Chem.* **389**, 905–918.
Matousek, J., Podzimek, T., Pouckova, P., Stehlik, J., Skvor, J., Lipovova, P. & Matousek, J. (2010). *Neoplasma*, **57**, 339–348.
Matousek, J., Podzimek, T., Poucková, P., Stehlík, J., Skvor, J., Soucek, J. & Matousek, J. (2009). *Oncol. Res.* **18**, 163–171.
Mueller, U., Darowski, N., Fuchs, M. R., Förster, R., Hellmig, M., Paithankar, K. S., Pühringer, S., Steffien, M., Zocher, G. & Weiss, M. S. (2012). *J. Synchrotron Rad.* **19**, 442–449.
Murshudov, G. N., Skubák, P., Lebedev, A. A., Pannu, N. S., Steiner, R. A., Nicholls, R. A., Winn, M. D., Long, F. & Vagin, A. A. (2011). *Acta Cryst.* D**67**, 355–367.
Olson, B. H. & Goerner, G. L. (1965). *Appl. Microbiol.* **13**, 314–321.
Otwinowski, Z. & Minor, W. (1997). *Methods Enzymol.* **276**, 307–326.
Pérez-Amador, M. A., Abler, M. L., De Rocher, E. J., Thompson, D. M., van Hoof, A., LeBrasseur, N. D., Lers, A. & Green, P. J. (2000). *Plant Physiol.* **122**, 169–180.
Podzimek, T., Matoušek, J., Lipovová, P., Poučková, P., Spiwok, V. & Šantrůček, J. (2011). *Plant Sci.* **180**, 343–351.
Romier, C., Dominguez, R., Lahm, A., Dahl, O. & Suck, D. (1998). *Proteins*, **32**, 414–424.
Sheldrick, G. M. (2008). *Acta Cryst.* A**64**, 112–122.
Soucek, J., Skvor, J., Poucková, P., Matousek, J., Slavík, T. & Matousek, J. (2006). *Neoplasma*, **53**, 402–409.
Trott, O. & Olson, A. J. (2010). *J. Comput. Chem.* **31**, 455–461.
Vagin, A. & Teplyakov, A. (2010). *Acta Cryst.* D**66**, 22–25.
Volbeda, A., Lahm, A., Sakiyama, F. & Suck, D. (1991). *EMBO J.* **10**, 1607–1618.
Weiss, M. S. (2001). *J. Appl. Cryst.* **34**, 130–135.
Winn, M. D. *et al.* (2011). *Acta Cryst.* D**67**, 235–242.